Contents list available at IJRED website

Int. Journal of Renewable Energy Development (IJRED)

Journal homepage: https://ijred.undip.ac.id

Research Article

Thermogravimetric Analysis and Kinetic Study on Catalytic Pyrolysis of Rice Husk Pellet using Its Ash as a Low-cost In-situ Catalyst

Wusana Agung Wibowo[a,b], Rochim Bakti Cahyono[b], Rochmadi[b], Arief Budiman[b,c,*]

[a]*Chemical Engineering Department, Universitas Sebelas Maret, Jl. Ir. Sutami 36A, Surakarta 57126, Indonesia*

[b]*Chemical Engineering Department, Universitas Gadjah Mada, Jl. Grafika 2, Yogyakarta 55284, Indonesia*

[c]*Center for Energy Studies, Universitas Gadjah Mada, Sekip K1A, Yogyakarta 55281, Indonesia*

Abstract. The thermogravimetric behaviors and the kinetic parameters of uncatalyzed and catalyzed pyrolysis processes of a mixture of powdered raw rice husk (RRH) and its ash (RHA) in the form of pellets were determined by thermogravimetric analysis at three different heating rates, i.e., 5, 10, and 20 K/min, from 303 to 873 K. This research aimed to prove that the rice husk ash has a catalytic effect on rice husk pyrolysis. To investigate the catalytic effect of RHA, rice husk pellets (RHP) with the weight ratio of RRH:ARH of 10:2 were used as the sample. Model-free methods, namely Friedman (FR), Kissinger-Akahira-Sunose (KAS), and Flynn-Wall-Ozawa (FWO), were used to calculate the apparent energy of activation (E_A). The thermogravimetric analysis showed that the decomposition of RHP in a nitrogen atmosphere could be divided into three stages: drying stage (303-443 K), the rapid decomposition stage (443-703 K), and the slow decomposition stage (703-873 K). The weight loss percentages of each stage for both uncatalyzed and catalyzed pyrolysis of RHP were 2.4-5.7%, 35.5-59.4%, and 2.9-12.2%, respectively. Using the FR, FWO, and KAS methods, the values of E_A for the degrees of conversion (α) of 0.1 to 0.65 were in the range of 168-256 kJ/mol for the uncatalyzed pyrolysis and 97-204 kJ/mol for the catalyzed one. We found that the catalyzed pyrolysis led the E_A to have values lower than those got by the uncatalyzed one. This phenomenon might prove that RHA has a catalytic effect on RHP pyrolysis by lowering the energy of activation.

Keywords: rice husk pellet, rice husk ash, pyrolysis, catalytic, thermogravimetric analysis

Article history: Received: 7th Oct 2021; Revised: 12th Nov 2021; Accepted: 18th Nov 2021; Available online: 24th Nov 2021
How to cite this article: Wibowo, W.A., Cahyono, R.B., Rochmadi, R. and Budiman, A. (2022). Thermogravimetric Analysis and Kinetic Study on Catalytic Pyrolysis of Rice Husk Pellet using Its Ash as a Low-cost In-situ Catalyst. *Int. J. Renew. En. Dev,* 11(1), 207-219.
https://doi.org/10.14710/ijred.2022.41887

1. Introduction

The energy development priority of a nation is targeted to achieve independence and security of national energy. Maximizing the use of new and renewable energy (NRE) for supplying energy demand by taking into account the economic level is commonly the major concern to reach the target. However, the utilization of NRE in Indonesia has only reached 2% of the total NRE potential. Meanwhile, Indonesia has various and abundant sources of biomass as an NRE alternative (Jamilatun *et al*., 2017a; Widiyannita *et al*., 2020). To overcome this imbalance, the government projects the use of biomass as an energy source to reach 22.7 million tons by 2050 (Yudiartono *et al*. 2018).

One of the most abundantly available biomass in Indonesia, as an agricultural country, is the solid waste of rice plantation or milling industries, which can produce about 200-300 kgs of husk waste per ton of dry milled grain. Indonesian Central Statistics Agency data in 2020 revealed that the national production of dry grain reached 10,929,840 tons. Based on the assumption that only 30% of the remaining husks are collectible, the country can produce rice husks about 3,278,952 tons. Furthermore, based on the calorific value of the rice husk in the range of 13-15 MJ/kg (Jenkins *et al*., 1998), the potential energy is 42,600 – 49,100 GJ in 2020.

Optimizing the use of rice husk as a renewable energy source through the thermochemical process (pyrolysis or gasification) is still an attractive alternative in future energy supplies. The process converts rice husks into gas and/or liquid that can be utilized directly as energy or a feedstock to produce valuable chemicals (Wang *et al*., 2018; Salman *et al*., 2018; Heryadi *et al*., 2019). Researchers have performed studies to ensure that the pyrolysis or gasification process produces more gas with low tar and high CO and H_2 contents. The use of catalyst has been widely studied in the last ten years because it plays a role in reducing the reaction temperature and increasing the efficiency of the gasification reaction, as well as encouraging tar cracking reactions, which can increase the amount of gas yielded and H_2 content (Rei *et al*., 1986). Recent studies focused on developing stable,

* Corresponding author: abudiman@ugm.ac.id

efficient, inexpensive, and reactive catalysts in the biomass pyrolysis and gasification process, referring to Parthasarathy & Narayanan (2014).

Catalysts that are widely used in the pyrolysis-gasification process of biomass are metal-based such as Ni, Fe, Zn, Cu, Co (Rei *et al*., 1986; Li *et al*., 2010; Fu *et al*., 2011; Shen *et al*., 2014b; Chen & Zhang, 2015; Shen *et al*., 2015; Prabahar *et al*., 2019). These catalysts are highly effective in increasing gas yield and H_2 content. Likewise, the use of acid-base mineral catalysts such as dolomite, zeolite, olivine, silica-alumina, $CaCO_3$, and $MgCO_3$ can upgrade the bio-oil quality, reduce tar and increase CO content (Rei *et al.,* 1986; Thakkar *et al*., 2016; Jamilatun *et al*., 2019; Yuan & Shen, 2019; Yuan *et al*., 2019).

Meanwhile, inexpensive catalysts such as char and ash are also applicable to the pyrolysis-gasification process. Char can reduce tar production and increase carbon conversion efficiency (Shen *et al*., 2014a; Shen *et al*., 2015), the amount of the gas yielded, and CO and H_2 contents in gas synthesis (Khonde *et al*., 2017). On the other hand, the use of rice husk ash with a high content of silica (SiO_2) and a wide area of the mesoporous surface as a catalyst in the rice husk pyrolysis can reduce the value of activation energy (Loy *et al*., 2018) and increase the quality and yield of bio-oil (Rong *et al*., 2018).

The in-situ catalytic pyrolysis-gasification process with the addition of rice husk ash has a limitation; it applies to a mixture of husk powder and husk ash only (Rong *et al*., 2018; Loy *et al*., 2018). Meanwhile, no researcher has studied the addition of ash as a catalyst into rice husk pellets as a raw material for the pyrolysis-gasification process. Thus, there have been no reports on the gas yielded and its composition. The catalytic reaction mechanism and the characteristics of the gas produced may be different when using powdered and pelletized materials. In this work, the pellet form was preferable to the original one because it, possibly, can yield a gas with a higher energy and H_2 and CO contents and has higher efficiency and stability of the process (Yoon *et al*., 2012).

In the evaluation of the pyrolysis reaction kinetics, the most common method for evaluating kinetic parameters can be classified into two major models, namely the model-fitting and the model-free. The use of these models will provide a suitable kinetic analysis as long as the calculation are based on the data obtained from the thermogravimetric analysis on multiple heating rates (Vyazovkin, 2021). In the model-fitting methods, various reaction models are tested to obtain the fit of the model with the experimental data. The most suitable model is then used to determine the single kinetic parameters for an overall process. These methods have several drawbacks, such as the inability to uniquely select the appropriate reaction model that poses inaccurate estimation (Azam *et al*., 2020), and not capable to represent the multi-step kinetics and complexity of solid-state reaction (Slopiecka *et al*., 2012; Heydari *et al*., 2015).

In contrast to the model-fitting methods, the model-free methods have the ability to avoid errors related to the choice of the reaction models (Yan *et al*., 2019). In these methods, the kinetic parameters were determined from various thermogravimetric curves at minimum three different heating rates having the same value of conversion. Moreover, the activation energy can be estimated in a wide range of temperatures and conversions (Azam *et al*., 2020). Therefore, the model-free methods are sometimes also known as the isoconversional methods. Furthermore, the model-free methods can be separated into two main types, namely the differential method (e.g Friedman method) and the integral methods (e.g Kissinger, Flynn-Wall-Ozawa, Kissinger-Akahira-Sunose, Miura-Maki). The advantage of the differential Friedman method is that it's not including the mathematical approximations of exponential integral that generating some errors. Therefore, some literature reported that Friedman method was considered as the accurate method to evaluate kinetic parameters (Heydari *et al*., 2015; Handawy *et al*., 2021). Meanwhile, the integral model-free methods are generated based on mathematical approximation of exponential integral which can enhance systematic error. More related to the integral methods, the Kissinger method does not calculate the activation energy at any conversions, but assumes that the activation energy is constant at all conversions (Heydari *et al*., 2015). This means that Kissinger method cannot reveal the complexity of the reaction. Furthermore the Kissinger-Akahira-Sunose method will give the same activation energy as the Miura-Maki method due to the similar curve plots. Meanwhile, the activation energy values will be different for Flynn-Wall-Ozawa method.

So far, there are no specific conclusions have been found to suggest that a particular isoconversional method is suitable for certain types of reacting solids (coal, biomass, plastics, etc.). Sometimes, the kinetic parameters presented in the literature vary significantly and quite confusing (Yan *et al*., 2019). Nevertheless, Friedman, Flynn-Wall-Ozawa, and Kissinger-Akahira-Sunose methods were considered as the better practice for determining the kinetic parameters from thermo-gravimetric data (Sarkar & Wang, 2020). Based on simplicity, better accuracy and often widely used of model-free (isoconversional) methods, the Friedman, Flynn-Wall-Ozawa, and Kissinger-Akahira-Sunose methods were chosen in this study to determine the kinetic parameters of the pyrolysis process.

This research aimed to study thermal analysis and catalytic pyrolysis kinetics of rice husk pellet added with its ash as a low-cost in-situ catalyst, and also to prove that rice husk ash has a catalytic effect on rice husk pyrolysis. Thermogravimetric analysis to obtain the kinetic parameters was performed using isoconversional methods, namely Friedman, Kissinger-Akahira-Sunose, and Flynn-Wall-Ozawa. The kinetic parameters obtained were then used to determine the thermodynamic parameters that represent the exchange of energy during a reaction, the system's potential energy, and the availability of the system in generating products.

2. Materials and Methods

2.1 Material and catalyst

The sun-dried rice husks in their original shape were obtained from a local rice mill in District Sukoharjo, Central Java, Indonesia, to be pulverized and sieved to get a particle size of -60+80 Tyler mesh (250-180 μm) to widen the reaction surface area. The powdered rice husks were then named raw rice husk (RRH). Meanwhile, its ash (RHA), to be the catalyst, was prepared by burning RRH in a muffle furnace at 1073 K for 60 minutes. The RHA produced was then cooled down to ambient temperature

and then kept in the closed glass container to be re-sieved to get a particle size of -60+80 Tyler mesh. Further, RRH and RHA with a weight ratio of 10:2 were then well mixed before densification in the form of pellets, produced by pressing such mixture by a hydraulic press machine under a tonnage of 1 ton for 5 minutes using a pellet mold with 3 mm in diameter. The rice husk pellets with that weight ratio were then coded as ARH20P. Meanwhile, those without the addition of ash were then coded as RRHP. The density (g/cm^3) of single pellet of RRHP and ARHP20 were found by measuring the diameter, length, and weight of individual pellet. The diameter and length of pellet were measured by using a standard srew micrometer, and the weight of pellet was measured using the Joanlab FA2204 analytical balance with the readability of 0.0001 g.

The proximate, ultimate, and calorific value analysis of RRH were conducted at the Center for Research and Development of Mineral and Coal Technology, Bandung, Indonesia. The proximate analysis was performed using a thermogravimetric analyzer (TA Instrument Q500) to determine the moisture content, volatile matter content, and ash content, whilethe fixed carbon was calculated by difference. The ultimate analysis was conducted with an elemental content analyzer (varioMICRO) to determine carbon, nitrogen, hydrogen, oxygen, and sulfur contents. Meanwhile, the calorific value of powdered rice husk RRH was measured using a bomb calorimeter (IKA C2000 basic). Furthermore, the crystalline phase analysis of RHA was done using X-ray diffraction (XRD) analyzer MD10 mini-diffractometer, MTI. Meanwhile, the surface topography and elemental content analysis were performed using scanning electron microscopy – energy dispersive X-ray (SEM-EDX) analyzer JEOL Benchtop SEM JCM7000. Those RHA characterizations were performed at the Center of Excellence for Electrical Energy Storage Technology, Universitas Sebelas Maret, Surakarta, Indonesia.

2.2 Thermogravimetric analysis

Thermogravimetric study of the RRHP and ARH20P pyrolysis processes was carried out at three heating rates 5, 10, 20 K/min with the absence and presence of the catalyst RHA using TGA-Differential Scanning Calorimetry (DSC) analyzer (Linseis STA PT1000). In each experiment, nitrogen gas (N_2) at a flow rate of 50 mL/min was introduced into the TGA for 30 minutes at 303 K to expel the unwanted oxidizer. Then, approximately 30 mg of RRHP or ARH20P was placed in a ceramic crucible (0.12 ml in volume) and then heated form 303 to 873 K in N_2 atmosphere. Finally, the samples were then kept constant at 873 K for 10 minutes to complete heating.

2.3 Kinetic study

The pyrolysis of solid is possibly represented in the one-step global model (Equation 1) that assumes that the changes of the sample weight can be observed (Jamilatun *et al*., 2017b; Loy *et al*., 2018). The discriptiom of biomass decomposition with this simple reaction model is determined based on certain reaction conditions by assuming a constant ratio of volatiles and char (Daniyanto *et al*., 2015; Pradana *et al*., 2019).

$$Biomass \xrightarrow{k} Volatiles + Char \quad (1)$$

In the above equation, volatiles refers to gas and tar (bio-oil), k is the apparent pyrolysis rate constant. By the thermal analysis using a thermogravimetric analyzer (TGA), the temperature and the change of the sample weight can be recorded. The conversion change of sample in regards to time, $d\alpha/dt$, depends on the rate constant that is dependent on temperature ($k(T)$) and also the differential model of reaction ($f(\alpha)$), expressed as:

$$\frac{d\alpha}{dt} = k(T)f(\alpha) \quad (2)$$

Or, in terms of integral reaction model ($g(\alpha)$), as follows:

$$g(\alpha) = k(T)t \quad (3)$$

where α, t, and T are the conversion, reaction time (minute), and temperature in Kelvin (K), respectively. The conversion, α, at any temperature for thermogravimetric analysis in non-isothermal condition, can be presented as the loss of sample weight (Loy *et al*., 2018), expressed as:

$$\alpha = \frac{m_i - m_t}{m_i - m_f} \quad (4)$$

where m_i, m_t, m_f are initial sample weight, sample weight at a certain time, and final sample weight remaining after a certain final temperature of the pyrolysis process. The dependence of reaction rate constant on temperature ($k(T)$) is represented in the Arrhenius formula below:

$$k(T) = Ae^{-\frac{E_A}{RT}} \quad (5)$$

where E_A is the apparent energy of activation (kJ/mol), R is the gas constant (8.314 J/K.mol), and A is the preexponential value (1/min). By substituting Equation (5) into Equation (2) and (3), the reaction rate expressions can be written as follow:

$$\frac{d\alpha}{dt} = Ae^{-\frac{E_A}{RT}}f(\alpha) \quad (6)$$

$$g(\alpha) = Ae^{-\frac{E_A}{RT}}t \quad (7)$$

For the non-isothermal process of solid-state kinetics, the heating rate equation, $\beta = \frac{dT}{dt}$ (K/min), was used to construct the model-free or iso-conversional kinetic model (Loy *et al*., 2018). Substitution of β into Equation (6) and (7) gives:

$$\beta\frac{d\alpha}{dT} = Ae^{-\frac{E_A}{RT}}f(\alpha) \quad (8)$$

$$g(\alpha) = \int_0^\alpha \frac{d\alpha}{f(\alpha)} = \frac{A}{\beta}\int_{To}^{T} e^{-\frac{E_A}{RT}}dT \quad (9)$$

In this study, the pyrolysis reaction was assumed to follow the first-order reaction model. Further, the differential and integral model can be expressed as:

$$f(\alpha) = (1-\alpha) \quad (10)$$

$$g(\alpha) = -\ln(1-\alpha) \quad (11)$$

2.3.1 Friedman (FR) Method

The basic assumption of the model-free (iso-conversional) method is that the activation energy remains the same at the same conversion value and independent of the temperature. And also, pyrolysis is defined to be a first-order reaction (Jiang & Wei, 2018). The most common iso-conversional differential method used to calculate the apparent energy of activation (E_A) is Friedman's method, which is obtained by derivation of Equation (8) followed by rearrangement that will give:

$$\ln\left(\beta\frac{d\alpha}{dT}\right) = \ln\left(Af(\alpha)\right) - \frac{E_A}{RT} \quad (12)$$

The straight line plot of $\ln\left(\beta\frac{d\alpha}{dT}\right)$ versus $\frac{1}{T}$ will give the slope which is then used to determine the E_A and the intercept which is used to obtain the A.

2.3.1 Flynn-Wall-Ozawa (FWO) Method

The FWO is the integral method for non-isothermal thermogravimetric analysis data which is derived from Equation (9):

$$g(\alpha) = \int_0^\alpha \frac{d\alpha}{f(\alpha)} = \frac{A}{\beta}\int_{To}^{T} e^{-\frac{E_A}{RT}}dT \approx \frac{A}{\beta}\int_0^T e^{-\frac{E_A}{RT}}dT = \frac{AE_A}{\beta R}p(u) \quad (13)$$

where $u = E/(RT)$ and $p(u)$ is the exponential integral expressed as $p(u) = 0.0048e^{-1.0516u}$ (Jiang & Wei, 2018). By substituting the exponential integral equation into Equation (13) and by taking the common logarithm, the following expression can be obtained:

$$\ln\beta = \ln\left(\frac{AE_A}{Rg(\alpha)}\right) - 5.331 - 1.052\frac{E_A}{RT} \quad (14)$$

The plot of $\ln\beta$ versus $\frac{1}{T}$ at the same α value for different heating rates (β) gives the slope and intercept that can be used to determine the E_A and A, respectively.

2.3.3 Kissinger-Akahira-Sunose (KAS) Method

The KAS method is integral and uses the different approximations of exponential integral, $p(u) = e^{-u}/u^2$ (Jiang & Wei, 2018). Substituting this exponential integral equation into Equation (13) and performing a logarithmic operation and also substituting $u = E/(RT)$ into the formula give the following equation:

$$\ln\left(\frac{\beta}{T^2}\right) = \ln\left(\frac{AR}{E_A g(\alpha)}\right) - \frac{E_A}{RT} \quad (15)$$

At selected α and β values, the estimated E_A and A values can be determined by the slope and intercept of the plot of $\ln(\beta/T^2)$ versus $\frac{1}{T}$, respectively.

Referring to Loy *et al.* (2018), the thermodynamic parameters, i.e., the enthalpy (ΔH), the Gibb's free energy (ΔG), and the entropy change (ΔS) can be determined by the E_A and A values from iso-conversional kinetic models. The relations are as follow:

$$\Delta H = E_A - RT \quad (16)$$

$$\Delta G = E_A + RT_m ln\left(\frac{K_B T_m}{hA}\right) \quad (17)$$

$$\Delta S = (\Delta H - \Delta G)/T_m \quad (18)$$

where:
K_B : Boltzman constant (1.381 x 10^{-23} J/K)
h : Plank constant (6.626 x 10^{-34} Js)
T_m : Peak temperature of DTG curve, K

The ΔH represents the exchange of energy during a reaction and the ΔG represents the increase of system's potential energy. Meanwhile, the ΔS represents the availability of the system in generating products.

3. Results and Discussion

3.1 Physico-chemical characterization of RRH and RHA

Based on the mesurements of pellet's diameter (D) and length (L) of three pieces of randomly selected pellets for each RRHP and ARHP20, we found that the ratio of L/D were in the range of 1.02-1.07. Meanwhile, the measured weight of the RRHP and ARHP20 were in the range of 28.0-30.1 mg and 29.4-35.1 mg, respectively. The calculated density of RRHP and ARHP20 were then found to be in the range of 1.019-1.029 g/cm^3 and 1.046-1.075 g/cm^3, respectively.

The results of the analysis of proximate, ultimate, and calorific values of RRH are presented in Table 1, in comparison with other results reported by previous researchers. The proximate analysis in air-dried basis (adb) showed that the moisture content in RRH had a similar value to those in the other results. In this study, there was no thermal pre-treatment for the RRH sample. The lowest moisture content in Loy *et al.* (2018) may be associated with the thermal pre-treatment of the sample before analysis. In general, thermochemical technologies require feedstocks with less than 15wt% moisture (Eke *et al.*, 2018). RRH sample with low moisture content is appropriate for feedstock of pyrolysis process and does not need for further thermal pre-treatment.

The volatile matter (VM) content in the RRH sample had a similarly high value as other results. According to Prakash & Sheeba (2016), this characteristic makes rice husks have high reactivity, thereby reducing the devolatilization temperature, which leads the thermal degradation process to be faster. However, high VM content tends to produce large amounts of tar during the thermochemical process.

The low H/O ratio and high VM content in rice husk tend to synthesis gas with low H_2 concentration and H_2/CO ratio (Gil *et al.*, 2019). The low nitrogen and sulfur contents in the RRH sample indicated the low emission of SO_2 and NOx that might be produced during the pyrolysis process. Furthermore, the higher heating value of RRH proved the potential for pyrolysis or gasification feedstock, which could generate sufficient heat required for small-scale application (Loy *et al.*, 2018). Another important chemical property for the thermochemical process of rice husks is the lignocellulosic composition. Cellulose and hemicellulose are the major abundant complex in rice husks. Lignin and silica are also found in rice husks (Abaide *et al.*, 2019). Rice husks contain cellulose, hemicellulose, and lignin about 32-39%, 19-22%, and 13-24%, respectively. All of them are active compounds that degrade thermally in the temperature range of 423-773 K. Thermal decomposition of hemicellulose, cellulose, and lignin are in the range of 423-623 K, 548-623 K, and 523-773 K, respectively.

Table 1
The proximate, ultimate, and calorific value analysis of RRH

Material and Property	References			
	This study (adb)	Loy *et al.* 2018	Rasool *et al.* 2018	Shen *et al.* 2015
PROXIMATE:				
Moisture (wt.%)	9.58	5.56	8.6	9.8
Volatile matter (wt.%)	58.26	57.55	60.55	59.3
Ash (wt.%)	18.16	14.68	12.85	20.5
Fixed Carbon (wt.%)	14.00	22.21	18.01	10.4
ULTIMATE:				
Carbon (wt.%)	35.24	38.47	38.33	37.9
Hydrogen (wt.%)	5.23	5.75	4.86	6.3
Nitrogen (wt.%)	0.33	1.68	2.25	0.4
Oxygen (wt.%)	40.97	54.09	54.31	55.3
Sulfur (wt.%)	0.066	< 0.01	0.25	0.1
HHV (MJ/kg)	14.01	15.49	9.68	-

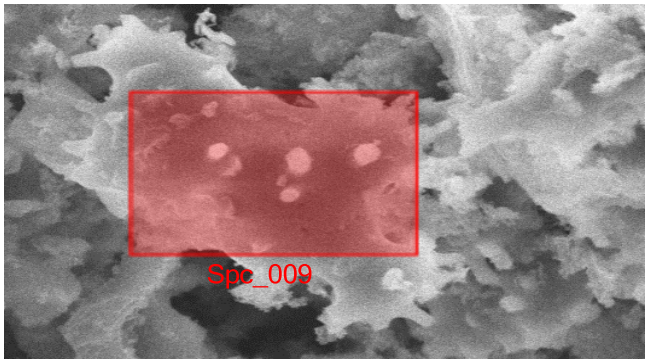

Fig. 1 SEM-EDX image of the catalyst RHA for 5000x magnification

The SEM-EDX analysis of the catalyst RHA was performed to get information about the elemental contents in rice husk ash. The SEM-EDX image for the RHA sample is shown in Figure 1, and the elemental composition of the RHA sample is shown in Table 2. The SEM-EDX spectra for only one point area will certainly not accurate to represent the measured sample. In this study, the result of the analysis can only provide a roughly information about the elemental contents of rice husk ash sample.

It can be seen in Table 2 that the RRH sample is rich in Si and O but has low K and Ca contents. Meawhile, the C content in RHA may be associated to the remaining unconverted carbon under the previously described ash production conditions. According to Prasara-A & Gheewala (2017), the high Si and O contents can be associated with the high SiO_2 content (around 90%) in the catalyst that possibly increases the surface area for reaction. Meanwhile, the presence of K and Ca oxide (e.g., K_2O and CaO) in the catalyst RHA can reduce the coke formation on its surface and assist in the activation of water (Sahrei *et al.*, 2017). Moreover, each of these metal compounds has particular catalytic effects and can promote the production of H_2 and CO_2, and also inhibit the production of CO, CH_4, C_2H_4, and C_6H_6 (Kajita *et al.*, 2010; Jiang *et al.*, 2015; Wang & Xiong, 2020). Daniyanto *et al.* (2015) also proved that the inorganic content of alkali and alkali earth metals (AAEMs) in biomass influence the rate of pyrolysis.

The XRD analysis was conducted to identify the crystalline phase of the catalyst RHA, the results of which are presented in Figure 2. The existing of the broad peaks are attributed to the typical amorphous charactheristic of material. The amorphous phase of material can be identified by the low value of cristallinity index (CI). In this study, the CI was calculated by using OriginPro® 2021 software based on XRD pattern data and it was found to be 30%. Based on Inorganic Crystal Structure Database (ICSD) provided by FIZ Karlsruhe for SiO_2, the peaks that are centered at 2θ of 22.15° and 70.57° in Figure 2 are attributed to the typical amorphous silica characteristic by the presence of the disordered cristobalite (SiO_2) (Shen *et al.*, 2015). The high content of nano-sized amorphous silica in rice husk ash contributes in CO_2 adsorption and increase the yield, namely hydrogen-rich synthetic gas (Shen *et al.*, 2014b).

Away from the ability to identify the crystalline phase, XRD analysis is possibly reveal the chemical composition information. It is interesting to know the types of K and Ca compounds which were caontained in RHA sample (see Table 2), since these elements have a catalysis effect on the thermochemical process. As reported in many studies, the K_2O and CaO compounds were found in the RHA. Therefore, these coumpounds were firstly choosen, beside SiO_2, to quantify their existence by matching the peaks of XRD pattern with their ICSD's XRD patterns (SiO_2: ICSD 170510; K_2O: ICSD 180571; CaO: ICSD 180198). As previously stated, the board peaks are dominated by SiO_2. While, the small peaks at 2θ of 32.03° and 37.16° may be attributed to CaO, and the other small peaks at 2θ of 48.61° and 56.76° may be attributed to K_2O. In general, it is quiet difficult to distinguish between the peaks that have low intensity and peaks that appear due to noises in the XRD pattern of amorphous materials. The more XRD pattern data should be provided and other possible compounds should be addressed to obtain an accurate results. However, this is beyond the scope of this paper.

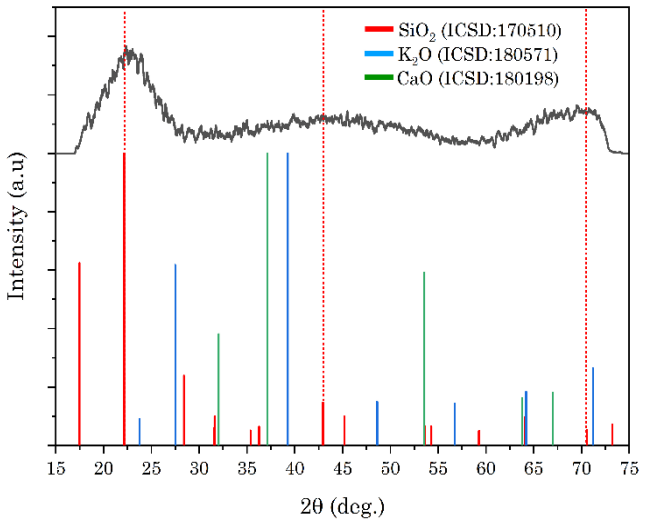

Fig. 2 The XRD pattern of the RHA at λ Cu K-α=1.564 Å

Table 2
Elemental compositions of RHA

Elements	SEM-EDX data	
	Mass %	Atom %
C	9.47±0.92	15.28±1.49
O	43.44±1.65	52.63±2.00
Si	45.00±1.03	31.06±0.71
K	1.83±0.28	0.91±0.14
Ca	0.26±0.13	0.12±0.06
Total	100.00	100.00

3.2 Thermogravimetric analysis

3.2.1 TG and DTG curves

The behaviors of thermal degradation of rice husk pellets with and without the addition of the catalyst RHA were investigated using a thermogravimetric analyzer (TGA) with the condition as explained in the methods. The thermogravimetric (TG) profile, which represents the weight loss behavior during the uncatalyzed and catalyzed pyrolysis processes in the heating rates of 5, 10, and 20 K/min, are shown in Figures 3a & 3b, respectively. In this study, weight loss (%) was calculated on a catalyst-free basis. Meanwhile, the differential thermogravimetric (DTG) profile during the uncatalyzed and catalyzed pyrolysis processes are shown in Figures 4a & 4b, respectively. The DTG curves were used to determine the initial, final, and peak decomposition temperatures. Peak temperature (T_m) is the temperature at which the weight loss rate (%/min) reaches the maximum.

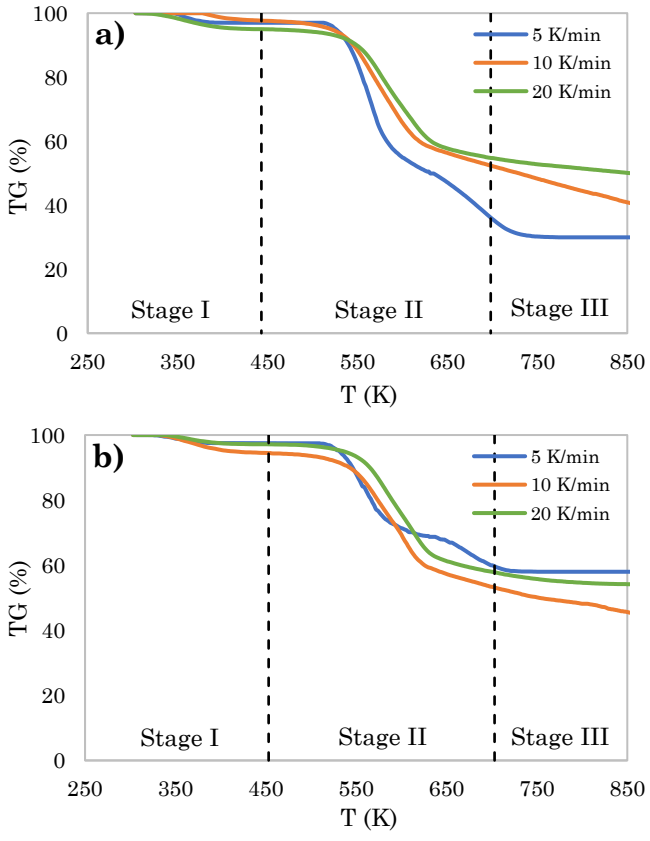

Fig. 3 TG curves of a) uncatalyzed pyrolysis of RRHP and b) catalyzed pyrolysis of ARH20P

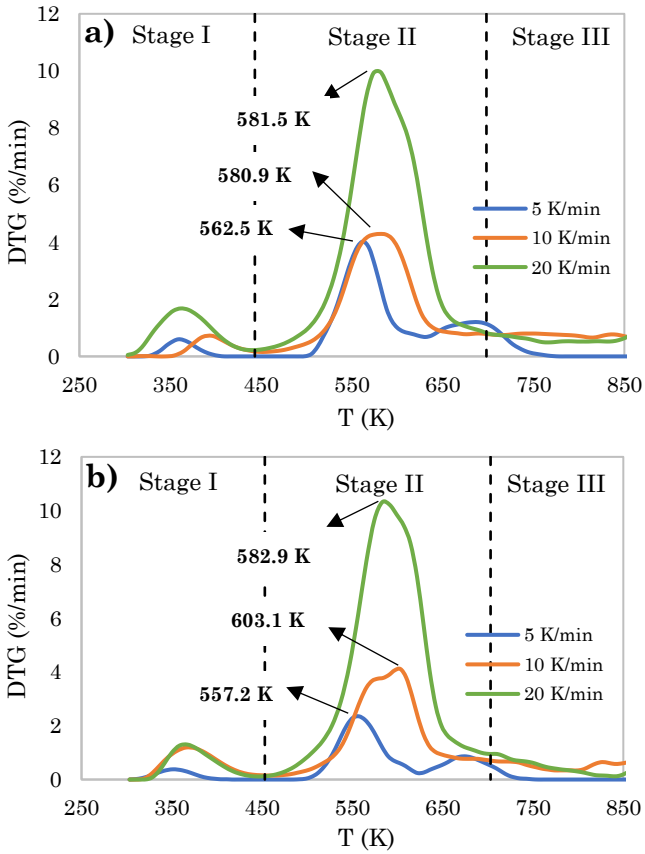

Fig. 4 DTG curves of a) uncatalyzed pyrolysis of RRHP and b) catalyzed pyrolysis of ARH20P

Based on TG and DTG curves, we found that the pyrolysis process was disparted into three stages in the range of temperature observation. Stage I was the first thermal degradation of RHP which represents the water vaporization at a low temperature range of 303-443 K.In Stage II, the curve showed the higher weight loss represents the devolatilization process took place. The steep slope of this TG curve was shown between the temperature range of 443-703 K which represents the thermal decomposition of hemicellulose and cellulose. Other fairly high weight loss can be seen in Stage III starting from 703 K to the final observed temperature of pyrolysis at 873 K, which represents the cellulose and mostly lignin decomposition (Quiroga *et al.*, 2009). In general, hemicellulose is decomposed at 473-588 K due to the high C=O compounds, while cellulose is decomposed at 588-673 K due to the presence of –OH and C-O functional groups with strong bonds. The high decomposition temperature of lignin is due to the strong bond of aromatics rings such as phenol and benzene structure (Loy *et al.*, 2018). Lignin, which is plenty of C=C and C-O-C stretching functional groups and aromatic structures is more stable to temperature than cellulose (Prandana *et al.* 2019) and requires a wider range of temperature to complete the decomposition.

The initial and final decomposition temperatures and the percentage of weight loss (on a catalyst-free basis) for the uncatalyzed and catalyzed pyrolysis of RHP in this study are presented in Table 3. The weight loss for RRHP (uncatalyzed) pyrolysis in Stages I, II, and III occurred in the range of 2.40-5.04%, 40.48-59.37%, and 5.52-12.25%, respectively.

Table 3
Data of temperature and weight loss of the uncatalyzed pyrolysis of RRHP and the catalyzed pyrolysis of ARH20P

Stage	Heating rate (K/min)	T initial (K)	T final (K)	Weight loss* (%)
RRHP (uncatalyzed)				
Stage 1	5	303.2	442.8	2.40
(drying)	10	303.2	447.2	2.40
	20	303.2	449.5	5.04
Stage 2	5	442.8	689.5	59.37
(rapid decomposition)	10	447.2	705.9	45.87
	20	449.5	705.1	40.48
Stage 3	5	689.5	868.5	6.93
(slow decomposition)	10	705.9	872.0	12.25
	20	705.1	875.6	5.52
Residue	5	-	-	31.30
	10	-	-	39.48
	20	-	-	48.97
ARH20P (catalytic)				
Stage 1	5	303.2	451.9	2.51
(drying)	10	303.2	457.9	5.66
	20	303.2	462.8	2.88
Stage 2	5	451.9	682.7	35.15
(rapid decomposition)	10	457.9	708.6	41.61
	20	462.8	710.2	39.69
Stage 3	5	682.7	874.2	2.89
(slow decomposition)	10	708.6	872.8	8.76
	20	710.2	870.8	3.65
Residue	5	-	-	59.45
	10	-	-	43.98
	20	-	-	53.78

Note: * catalyst-free basis

Meanwhile, the weight loss for ARH20P (catalyzed) pyrolysis in Stages I, II, and III occurred in the range of 2.51-5.66%, 35.15-41.61%, and 2.89-8.76%, respectively. The range of mass loss obtained in this study was in a good agreement with the results reported by Loy *et al*. (2018). The mass loss in Stage III can be higher if the final temperature of pyrolysis is increased. In addition, the weight loss percentage at each stage on RRHP pyrolysis at 10 K/min was also in a good agreement with the results obtained by Guo *et al*. (2020). Also shown in Table 3, the final residue of the catalyzed pyrolysis of ARH20P was higher than that of the uncatalyzed pyrolysis of RRHP, possibly affected by the addition of the fairly high weight of the catalyst. The highest weight loss in Stage II represents the most active zone, for that reason, we decided to study kinetics at this stage.

The profiles of TG and DTG of the uncatalyzed pyrolysis catalyzed pyrolysis of RHP shown in Figures 3 & 4 showed similar trends. The maximum peak of decomposition of the catalyzed pyrolysis at the heating rate of 20 K/min is higher than those of the uncatalyzed on. This finding was in contrast with the maximum decomposition peak of a catalyzed pyrolysis at a heating rate of 5 K/min that was lower than those for uncatalyzed pyrolysis. Meanwhile, the maximum decomposition peak of catalyzed pyrolysis was slightly lower than those for uncatalyzed pyrolysis at a heating rate of 10 K/min. The maximum decomposition rate had decreased by 7.7% and 41.8% at 10 K/min and 5 K/min, respectively. This finding was in line with the reports by previous studies that catalyzed pyrolysis of biomass can decrease the rate of maximum decomposition and the duration of thermal decomposition (Loy *et al*., 2018; Xiang *et al*., 2018).

Further discussion to the DTG curve profiles was related to the superimposition of DTG curves that were observed in Stage II and Stage III, especially at the heating rates of 10 K/min and 20 K/min. The lower mass loss rate (lower DTG curve) at higher heating rate (20 K/min) were observed. This phenomenon may related to the significant difference between the observed temperature and the actual pellet temperature. In this case, the heat transfer plays an important role. The significant increase of observed temperature due to the higher heating rate program was not accompanied by the significant increase of pellet temperature. Therefore, even though the observed temperature was high, the solid mass loss rate or solid conversion remained low. The superimposed DTG curve can lead the wrong results of kinetic parameters since the kinetic models that are used in calculation require thermogravimetric analysis data on multiple heating rates.

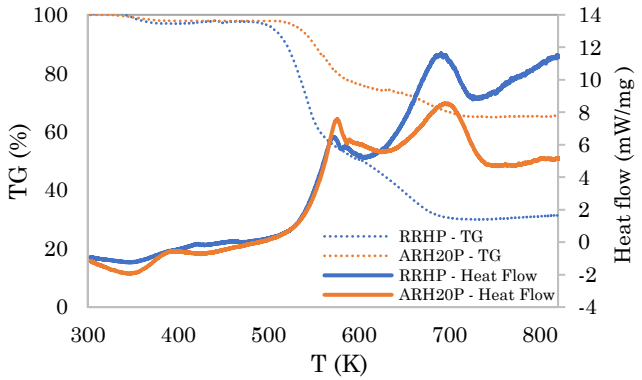

Fig. 5 DSC curve for the pyrolysis of RRHP and ARH20P at the heating rate of 5 K/min

3.2.2 DSC curves

DSC can be used to track the changes in heat flow to and from a sample with respect to temperature changes in a TGA equipment. Thus, it can be used to investigate wheter the process is exothermic or endothermic. The DSC curve for the pyrolysis of RRHP and ARH20P at the heating rate of 5 K/min are shown in Figure 5. The negative peak of DSC curve indicates an endothermic process, while the positive peak indicates the exothermic process (Jamilatun *et al*., 2017b; Pradana *et al*., 2019). The negative peak was found in the drying stage beetween 300-400 K that represents the absorption of heat for moisture release. After the drying stage, all processes that occur were exothermic processes as evidenced by positive peaks. This phenomenon was also observed for pyrolysis of RRHP and ARH20P at heating rates of 10 K/min and 20 K/min. The devolatilization stage is an exothermic process as a result of fragmentation, cracking, reforming, polymerization, and dehydration reactions of RRH components (hemicellulose, cellulose, and lignin) which are all exothermic. This result is in agreement with the result obtained by Said *et al*. (2014) and Rasool *et al*. (2018).

The exothermic process can be attributed to the increase in enthalpy which is generated during the devolatilization stage. This enthalpy of reaction is possibly calculated from DSC curve by calculating the existing peaks area through integration of the heat flow (mW/mg or J/g.s) with time (s). The calculations were conducted by using OriginPro® 2021 software, and we found that the enthalpy of reaction were to be 4,026 J/g and 4.181 J/g for pyrolysis of RRHP and ARH20P, respectively. The values were close to the enthalpy of reaction of rice husk pyrolysis in the N_2 atmosphere as reported by Said *et al*. (2014).

3.3 Kinetic analysis

The kinetic parameters were investigated using iso-conversional models, namely Friedman (FR), Kissinger-Akahira-Sunose (KAS), and Flynn-Wall-Ozawa (FWO). In this study, Stage II as an active zone of the pyrolysis was reviewed for the following kinetic study of RHP with experimental data taken at heating rates of 5, 10, and 20 K/min. The plot of $\ln(\beta\, d\alpha/dT)$ versus $1/T$ of the FR model, that of $\ln\beta$ versus $1/T$ of the FWO model, and that of $\ln(\beta/T^2)$ versus $1/T$ of the KAS model at the same α value for different heating rates (β) for uncatalyzed and catalyzed pyrolysis are shown in Figures 6a & 6b, respectively. The kinetic parameters values, E_A, and A were then calculated by the slope and intercept of the curves. The results are shown in Table 4. The selected α values in the kinetic study of dry sample were in the range of 0.1–0.65, indicating the decomposition of hemicellulose, cellulose, and lignin contents in RHP. As presented in Table 4, the values of E_A and A varied, depending on α values. The fluctuating values of the kinetic parameters showed that the reaction mechanism varied along with the active zone temperature of pyrolysis.

To evaluate the accuracy of the fitted line, the regression coefficient (R^2) was then used in this study. We found that the calculated mean of R^2 was more than 90%, indicating good precision and significance of the models. The E_A values of uncatalyzed pyrolysis of RRHP by the FR, FWO, and KAS methods were in the range of 168-256 kJ/mol, 179-239 kJ/mol, and 178-242 kJ/mol, respectively. Meanwhile, the E_A values of catalyzed pyrolysis of ARHP20 by the FR, FWO, and KAS methods were in the range of 97-159 kJ/mol, 110-202 kJ/mol, and 106-204 kJ/mol, respectively. As shown in Table 3, the mean E_A value for FWO and KAS were in closer results (206 and 207 kJ/mol, respectively) compared to FR (191 kJ/mol) for uncatalyzed pyrolysis of RRHP. In the catalyzed pyrolysis of ARHP20, the FWO and KAS also produced closer results to mean E_A (133 and 130 kJ/mol, respectively) compared to FR (112 kJ/mol). This finding was in accordance with the results reported by prevous studies (Sarkar & Wang, 2020; Cepeliogullar *et al*., 2016), that the FWO and KAS models provided close E_A values. Moreover, for all methods, the range and mean value of E_A of ARHP20 were lower than those of RRHP. These results agreed with those of Loy *et al*. (2018), that the E_A values determined in catalyzed pyrolysis of RHP by the addition of RHA as the catalyst were lower than those of pyrolysis of RHP without the addition of RHA.

The addition of the catalyst RHA lowered the E_A values, possibly caused by an increase in the rate of a secondary reaction (Loy *et al*., 2018). The rice husk molecules difused over the pores of the catalyst, then the remaining char and metal oxides in it would further accommodate the decomposition reaction. The cost-free preparation of RHA and the ability to lower E_A values suggest that RHA is an inexpensive and suitable catalyst for the pyrolysis of RHP, although not as effective as metal-based catalysts.

In the review of the pre-exponential (A) value, the similar findings were also encountered that the A values for FWO and KAS were in closer results compared to FR. This finding has been applied to both the uncatalyzed pyrolysis of RRHP and the catalyzed pyrolysis of ARHP20. On the other hand, the variations in A values indicate the complex composition of the RHP sample and the complexity of the reactions during decomposition (Kaur *et al*., 2018). The A value less than 10^{10} (1/min) means that the reaction was occurring on the surface or as a closed complex reaction. It is associated with the water molecules loss in which the reactants (hemicellulose, cellulose, and lignin) and the activated complex (the component's structure at the maximum energy along the reaction pathway) can freely rotate.

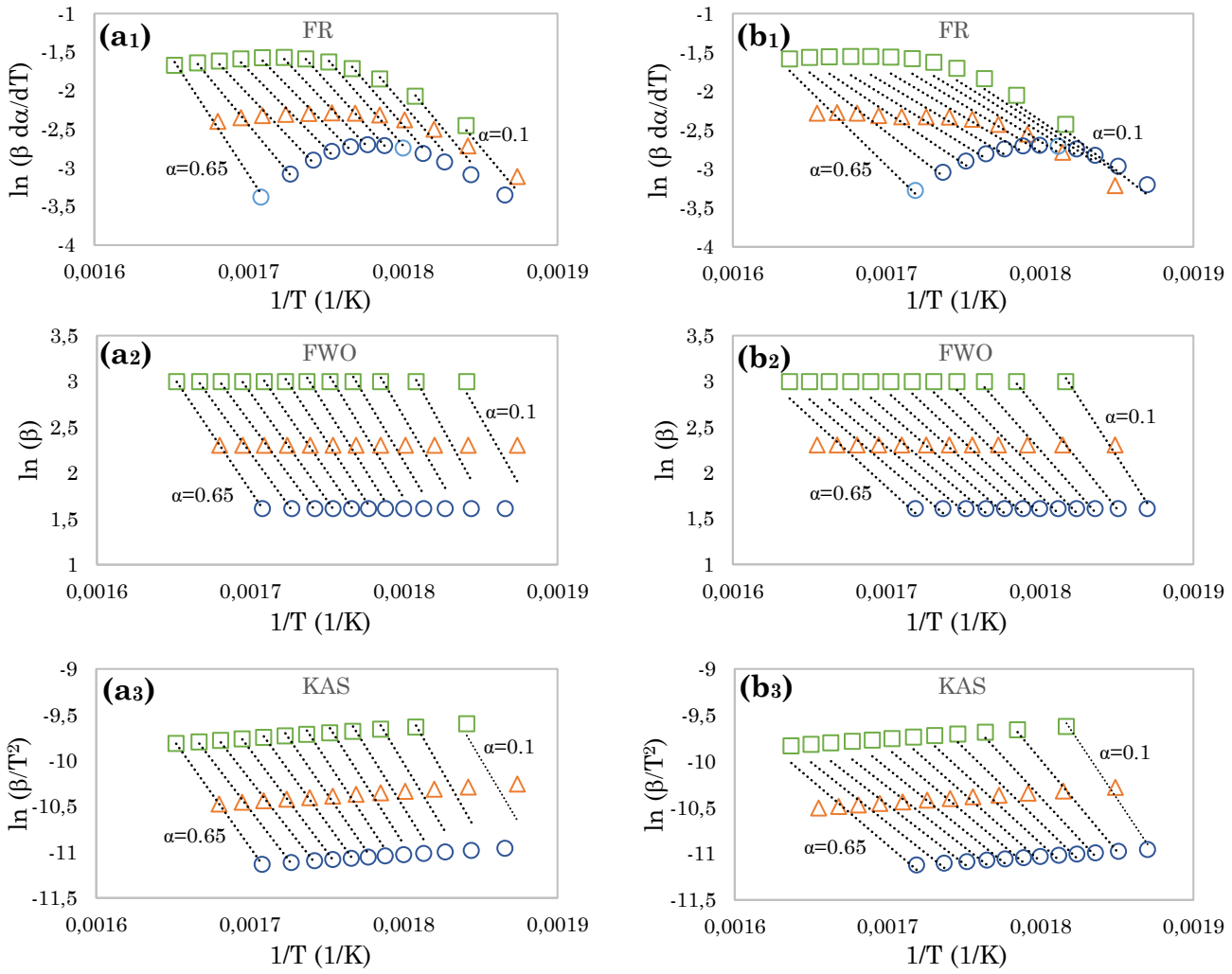

Fig. 6 Model-free kinetic plots of a) uncatalyzed pyrolysis of RRHP and b) catalyzed pyrolysis of ARH20P. Subscripts 1, 2, and 3 denote FR, FWO, and KAS, respectively. Marker: ○ 5 K/min, Δ 10 K/min, □ 20 K/min

According to Turmanova (2008); Xu & Chen (2013), if the *A* values are to increase to the range of 10^{10} to 10^{11} (1/min), then a simple complex is possible to react where the reactants can freely rotate, different from an activated complex. Meanwhile, an *A* value greater than 10^{11} (1/min) indicates a complex reaction where the activated complex and the starting reactants are probably limited to rotate, explaining that the system is already occupied by molecules, one of which has a high degree of disposition.

This study showed that the *A* value in the active zone of uncatalyzed pyrolysis gradually decreased from α = 0.1 to 0.55. Attention was drawn to the decomposition hemicellulose and cellulose contents in RHP. In the α range of 0.55 to 0.65, the *A* value tended to increase, indicating that lignin in RHP started to decompose. In this term, the *A* value was above 10^{13} (1/min), indicating the occurrence of a complex reaction, requiring a high E_A. However, the addition of RHA to the RHP decreased the *A* value to below 10^{10} (1/min). This phenomenon implied that RHA could shift the complex reaction to a semi-complex reaction, thus requiring less E_A (Loy *et al.*, 2018).

In comparing of the three models based on the average value of R^2 in Tabel 4, it was found that the accuracy of the models followed the order of FR>FWO>KAS for uncatalyzed pyrolysis of RRHP. However, the value of R^2 for all three models were close enough and still quite accurate with R^2>0.9. Meanwhile, for the catalyzed pyrolysis of ARHP20, the accuracy of the models followed the order of FWO>KAS>FR with a significant difference for FR when compared to others. It seems to be noted that the FR was not an accurate model to represent the kinetics of catalytic pyrolysis of ARH20P due to the low value of R^2. Based on that descriptions, it can be concluded that the FWO and KAS models can be selected as the suitable models to represent the kinetics of both uncatalyzed pyrolysis of RRHP and catalyzed pyrolysis of ARHP20. For further studies, the applicability of the models needs to be tested at different temperatures and heating rates.

In addition to the E_A and *A* values, some of thermodynamic parameters such as enthalpy (ΔH), change of entropy (ΔS), and Gibb's free energy (ΔG) for uncatalyzed and catalyzed pyrolysis of RHP at 20 K/min

are presented in Table 5. Ethalpy is the quantity of energy delivered in a chemical reaction. The average enthalpy values were found to be in the range of 188-203 kJ/mol and 107-128 kJ/mol for pyrolysis of RRHP and ARH20P, respectively. The ontained results were close enough to the enthalpy of RH pyrolysis reported by Loy *et al.* (2018).

In this study, by comparing the ΔH and E_A values of uncatalyzed and catalyzed pyrolysis of RHP, there was a low barrier of potential energi (~5 kJ/mol), which reflected the viability of the reaction to undergo the pyrolysis condition. The smaller the difference between ΔH and E_A, the more favorable the occurrence of the reaction.

Gibb's free energy (ΔG) describes the total increase in the system's potential energy as the reactants moved closer together and an activated complex was formed. The results of the calculation of ΔG of uncatalyzed and catalyzed pyrolysis of RHP were in the range of 177–198 kJ/mol and 182–196 kJ/mol, respectively. These values are close to the results found by Loy *et al.* (2018). As shown in Table 5, the more positive the ΔS values throughout the degree of conversion obtained for uncatalyzed pyrolysis of RHP, the greater the disorder of RHP and the lower the system availability generate products. However, the catalyzed pyrolysis of RHP with the addition of the catalyst RHA showed a distinct trend in ΔS values, almost all of which are negative, representing a low degree of disorder of the products compared to the starting reactants. It also indicated that less reactivity was required so that more quantity of volatiles could be easily formed on the active surface of RHA, which decreased the disorderdegree of products. A similar trend was also reported by previous studies, in which the ΔS values changed from positive to negative after the addition of catalyst (Loy *et al.*, 2018; Rasool *et al.*, 2018).

Table 4
The apparent energy of activation (E_A) and pre-exponential value (A) of uncatalyzed pyrolysis of RRHP and catalyzed pyrolysis of ARH20P using the model-free methods

α	FR			FWO			KAS		
	E_A (kJ/mol)	A (1/min)	R^2	E_A (kJ/mol)	A (1/min)	R^2	E_A (kJ/mol)	A (1/min)	R^2
RRHP (uncatalyzed)									
0.10	195.49	9.36E+15	0.76	226.87	2.07E+19	0.51	229.71	3.51E+19	0.49
0.15	199.70	1.80E+16	0.90	239.50	2.46E+20	0.79	242.84	4.52E+20	0.78
0.20	194.75	4.86E+15	0.95	228.62	1.57E+19	0.88	231.29	2.56E+19	0.87
0.25	191.38	1.90E+15	0.98	221.35	2.46E+18	0.93	223.57	3.69E+18	0.92
0.30	187.32	6.52E+14	0.99	215.24	5.21E+17	0.96	217.06	7.26E+17	0.95
0.35	181.45	1.52E+14	1.00	208.18	9.20E+16	0.98	209.57	1.18E+17	0.97
0.40	174.99	3.19E+13	1.00	201.05	1.63E+16	0.99	202.00	1.92E+16	0.99
0.45	169.72	8.61E+12	0.99	192.67	2.24E+15	1.00	193.12	2.39E+15	1.00
0.50	168.08	4.97E+12	0.99	185.15	3.78E+14	1.00	185.14	3.65E+14	1.00
0.55	174.51	1.49E+13	0.99	179.14	8.86E+13	1.00	178.75	7.88E+13	1.00
0.60	198.44	1.50E+15	1.00	181.56	1.21E+14	1.00	181.21	1.08E+14	1.00
0.65	256.14	1.19E+20	0.99	197.58	2.63E+15	1.00	197.96	2.75E+15	1.00
Average	191.00	9.92E+18	0.96	206.41	2.38E+19	0.92	207.69	4.31E+19	0.91
ARH20P (catalyzed)									
0.10	127.74	1.99E+09	0.84	202.51	5.10E+16	0.99	204.02	6.78E+16	0.98
0.15	112.29	6.63E+07	0.85	165.66	9.78E+12	1.00	165.13	8.38E+12	1.00
0.20	107.47	2.31E+07	0.86	148.56	2.02E+11	0.98	147.05	1.36E+11	0.98
0.25	103.60	9.77E+06	0.85	137.55	1.74E+10	0.97	135.40	9.78E+09	0.97
0.30	101.72	6.20E+06	0.84	129.89	3.19E+09	0.96	127.27	1.57E+09	0.95
0.35	99.85	3.92E+06	0.82	124.21	9.13E+08	0.94	121.23	4.04E+08	0.93
0.40	97.83	2.38E+06	0.80	119.54	3.25E+08	0.93	116.24	1.31E+08	0.92
0.45	98.63	2.59E+06	0.80	115.42	1.31E+08	0.92	111.84	4.81E+07	0.90
0.50	101.90	4.68E+06	0.82	112.15	6.30E+07	0.90	108.33	2.15E+07	0.88
0.55	110.96	2.74E+07	0.86	110.83	4.56E+07	0.89	106.87	1.50E+07	0.88
0.60	126.61	5.84E+08	0.91	112.18	5.69E+07	0.89	108.20	1.88E+07	0.88
0.65	159.29	3.49E+11	0.95	119.94	2.57E+08	0.90	116.28	9.57E+07	0.88
Average	112.32	2.93E+10	0.85	133.20	4.25E+15	0.94	130.66	5.65E+15	0.93

Table 5
Enthalpy, Gibb's free energy, and entropy of uncatalyzed pyrolysis of RRHP and catalyzed pyrolysis of ARH20P at 20 K/min

α	FR			FWO			KAS		
	ΔH (kJ/mol)	ΔG (kJ/mol)	ΔS (kJ/mol.K)	ΔH (kJ/mol)	ΔG (kJ/mol)	ΔS (kJ/mol.K)	ΔH (kJ/mol)	ΔG (kJ/mol)	ΔS (kJ/mol.K)
RRH (uncatalyzed)									
0.10	190.97	183.14	0.01	222.35	177.28	0.08	225.19	177.57	0.08
0.15	195.10	184.19	0.02	234.90	177.95	0.10	238.24	178.35	0.10
0.20	190.09	185.57	0.01	223.96	180.37	0.07	226.63	180.68	0.08
0.25	186.68	186.74	0.00	216.65	182.06	0.06	218.87	182.32	0.06
0.30	182.57	187.85	-0.01	210.49	183.46	0.05	212.31	183.67	0.05
0.35	176.66	189.02	-0.02	203.39	184.78	0.03	204.78	184.97	0.03
0.40	170.16	190.11	-0.03	196.22	186.02	0.02	197.17	186.17	0.02
0.45	164.86	191.17	-0.05	187.81	187.23	0.00	188.26	187.37	0.00
0.50	163.18	192.18	-0.05	180.25	188.31	-0.01	180.24	188.47	-0.01
0.55	169.56	193.31	-0.04	174.19	189.32	-0.03	173.80	189.49	-0.03
0.60	193.45	194.94	0.00	176.57	190.23	-0.02	176.22	190.43	-0.02
0.65	251.11	198.10	0.09	192.55	191.36	0.00	192.93	191.53	0.00
Average	188.73			201.61			202.89		
ARH20 (catalyzed)									
0.10	123.16	189.83	-0.11	197.93	181.92	0.03	199.44	182.05	0.03
0.15	107.63	190.86	-0.14	161.00	186.55	-0.04	160.47	186.77	-0.05
0.20	102.76	191.15	-0.15	143.85	188.26	-0.08	142.34	188.66	-0.08
0.25	98.84	191.45	-0.16	132.79	189.13	-0.10	130.64	189.77	-0.10
0.30	96.92	191.78	-0.16	125.09	189.69	-0.11	122.47	190.50	-0.12
0.35	95.01	192.13	-0.17	119.37	190.07	-0.12	116.39	191.04	-0.13
0.40	92.95	192.53	-0.17	114.66	190.41	-0.13	111.36	191.51	-0.14
0.45	93.71	192.92	-0.17	110.50	190.69	-0.14	106.92	191.97	-0.15
0.50	96.94	193.32	-0.17	107.19	190.97	-0.14	103.37	192.36	-0.15
0.55	105.96	193.81	-0.15	105.83	191.22	-0.15	101.87	192.64	-0.16
0.60	121.57	194.64	-0.13	107.14	191.49	-0.14	103.16	192.88	-0.15
0.65	154.21	196.34	-0.07	114.86	191.95	-0.13	111.20	193.07	-0.14
Average	107.47			128.35			125.80		

4. Conclusion

The thermal decomposition behaviors and kinetic parameters in the uncatalyzed and catalyzed pyrolysis of rice husk pellets (RHP) were successfully investigated. The thermogravimetric analysis showed that the thermal decomposition of RHP in a nitrogen atmosphere could be divided into three stages: drying stage (303-443 K), the high heating rate pyrolysis stage (443-703 K), and the low heating rate pyrolysis stage (703-873 K). The weight loss percentage of each stage for both uncatalyzed and catalyzed pyrolysis of RHP were 2.4-5.7%, 35.5-59.4%, and 2.9-12.2%, respectively. Using the FR, FWO, and KAS methods, the values of E_A for the degrees of conversion (α) of 0.1 to 0.65 were in the ranges of 168-256 kJ/mol and 97-204 kJ/mol for the uncatalyzed and catalyzed pyrolysis, respectively. We found that the catalyzed pyrolysis of RHP led to an E_A value lower than the uncatalyzed pyrolysis did. This phenomenon might prove that RHA has a catalysis effect on RHP pyrolysis by lowering the energy of activation.

Acknowledgments

The authors gratefully thank the Directorate General of Higher Education, Ministry of Research Technology and Higher Education, the Republic of Indonesia for the support and funding.

References

Azam, M., Ashraf, A., Jahromy, S.S., Raza, W., Khalid, H., Raza, N., Winter, F.(2020). Isoconversional nonisothermal kinetic analysis of municipal solid waste, refuse-derived fuel, and coal. *Energy Science & Engineering, 8*, 3728–3739; https://doi.org/10.1002/ese3.778

Cepeliogullar,)., Haykiri-Acma, H., Yaman, S. (2016). Kinetic modelling of RDF pyrolysis: model-fitting and model-free approaches. *Waste Management, 48*, 275-284; http:// dx.doi.org/10.1016/j.wasman.2015.11.027

Chen, Z. & Zhang, L. (2015). Catalyst and process parameters for the gasification of rice husk with pure CO_2 to produce CO. *Fuel Processing Technology, 133,* 227-231; doi.org/ 10.1016/j.fuproc.2015.01.027

Daniyanto, Sutijan, Deendarlianto, and Budiman, A. (2015). Effect of dry torrefaction on kinetics of catalytic pyrolysis of sugarcane bagasse. Presented on International Conference of Chemical and Material Engineering (ICCME) 2015. *AIP Conference Proceedings, 1699*, 030017; dx.doi.org/ 10.1063/1.4938302

Eke, J., Onwudili, J.A., Bridgwater, A.V. (2018). Influence of moisture contents on the fast pyrolysis of Trommel Fines in a bubbling bed reactor. *Waste and Biomass Valorization*; doi.org/10.1007/s12649-018-00560-2

Fu, P., Yi, W., Bai, X., Li, Z., Cai, H., Hu, S., & Xiang, J. (2011). Research on catalytic gasification characteristics and reaction kinetics of rice husk. Asia-Pacific Power and Energy Engineering Conference, APPEEC 2011, Article number 5748763; doi.org/10.1109/appeec.2011.5748763

Gil, M.V., Gonzalez-Vasquez, M.P., Garcia, R., Rubiera, F., Pevida, C. (2019). Assessing the influence of biomass properties on the gasification process using multivariate data analysis. *Energy Conversion and Management, 184,* 649-660; doi.org/10.1016/j.enconman.2019.01.093

Guo, G., Zhang, K., Liu, C., Xie, S., Li, X., Li, B., Shu, J., Niu, Y., Zhu, H., Ding, M., Zhu, W. (2020). Comparative investigation on thermal decomposition of powdered pelletized biomasses: Thermal conversion charactheristics and apparent kinetics. *Bioresource Technology, 301*, 122732, 1-9; doi.org/10.1016/j.biortech.2020.122732

Heryadi, R., Uyun, A.S., Nur, S.M., and Abdullah, K. (2019). Single-stage dimethyl ether plant model based on gasification of palm empty fruit bunch. IOP Conf. Series: *Materials Science and Engineering 532* (2019) 012009; doi.org/10.1088/1757-899X/532/1/012009

Heydari, M., Rahman, M., Gupta, R. (2015). Kinetic study and thermal decomposition behavior of lignite coal. *International Journal of Chemical Engineering 2015*, Article ID 481739. http://dx.doi.org/10.1155/2015/481739

Jamilatun, S., Budiman, A., Budhijanto, Rochmadi. (2017a). Non-catalytic slow pyrolysis of Spirulina Platensis residue for production of liquid biofuel. *International Journal of Renewable Energy Research, 7 (4)*, 1901-1908; ISSN: 1309-0127

Jamilatun, S., Budhijanto, Rochmadi and Budiman, A. (2017b). Thermal decomposition and kinetic studies of pyrolysis of *Spirulina platensis* residue. *International Journal of Renewable Energy Development, 6* (3), 193-201; doi.org/ 10.14710/ijred.6.3.193-201

Jamilatun, S., Budhijanto, Rochmadi, Yuliestyan, A., Budiman, A. (2019). Effect of grain size, temperature and catalyst amount on pyrolysis products of Spirulina Platensis residue (SPR). *International Journal of Technology, 10 (3)*, 541-550; dx.doi.org/10.14716/ijtech.v10i3.2918

Jenkins, B.M., Baxter, L.L., Miles Jr., T.R., Miles, T.R. (1998). Combustion properties of biomass. *Fuel Processing Technology, 54,*17-46;doi.org/10.1016/S0378-3820(97)00059-3

Jiang, G. and Wei, L. (2018). Phase Change Materials and Their Application, Chapter 8: Analysis of pyrolysis kinetic model for processing of thermogravimetric analysis data, pp 143-163; dx.doi.org/10.5772/intechopen.79226.

Jiang, L., Hu, S., Wang, Y., Su, S., Sun, L., Xu, B., He, L., Xiang, J. (2015). Catalytic effects of inherent alkali and alkaline earth metallic species on steam gasification of biomass. *International Journal of Hydrogen Energy, 40,* 15460-15469; doi.org/10.1016/j.ijhydene.2015.08.111

Kajita, M., Kimura, T., Norinaga, K., Li, C., Hayashi, J. (2010). Catalytic and noncatalytic mechanisms in steam gasification of char from the pyrolysis of biomass. *Energy & Fuels, 24*, 108-116; doi.org/10.1021/ef900513a

Kaur, R., Gera, P., Jha, M.K., Bhaskar, T. (2018). Pyrolysis kinetics and thermodynamic parameters of castor (Ricinus communis) residue using thermogravimetric analysis. *Bioresources Technology, 250*, 422–428; doi.org/10.1016/ j.biortech.2017.11.077

Khonde, R., Nanda, J., Chaurasia, A. (2017). Experimental investigation of catalytic cracking of rice husk tar for hydrogen production. *Journal of Material Cycles and Waste Management, 20* (2), 1310-1319; doi.org/ 10.1007/s10163-017-0695-0

Li, J., Liu, J., Liao, S., Yan, R. (2010). Hydrogen-rich gas production by air-steam gasification of rice husk using supported nano-NiO/γ-Al2O_3 catalyst. *International Journal of Hydrogen Energy, 35*, 7399-7404; doi.org/10.1016/ j.ijhydene.2010.04.108

Loy, A.C.M., Gan, D.K.W., Yusup, S., Chin, B.L.F., Lam, M.K., Shahbaz, M., Unrean, P., Acda, M.N., and Rianawati, E. (2018). Thermogravimetric kinetic modeling of in-situ catalytic pyrolytic conversion of rice husk to bioenergy using rice hull ash catalyst. *Bioresource Technology, 261*, 213-222; doi.org/10.1016/j.biortech.2018.04.020

Parthasarathy, P. and Narayanan, K.S. (2014). Hydrogen production from steam gasification of biomass: influence of process parameters on hydrogen yield – A review. *Renewable Energy, 66,* 570-579; doi.org/10.1016/j.renene.2013.12.025

Prabahar, R.S.S., Nagaraj, H., Jeyasubramanian, K. (2019). Enhanced recovery of H2 gas from rice husk and its char enabled with nano catalytic pyrolysis/gasification. *Microchemical Journal, 146*, 922-930; doi.org/10.1016/ j.microc.2019.02.024

Pradana, Y.S., Daniyanto, Hartono, M., Prasakti, L., Budiman, A. (2019). Effect oc calcium and magnesium catalyst on pyrolysis kinetic of Indonesian sugarcane bagasse for biofuel production. *Energy Procedia, 158*, 431-439; doi.org/ 10.1016/j.egypro.2019.01.128

Prakash, P., & Sheeba, K. N. (2016). Prediction of pyrolysis and gasification characteristics of different biomass from their Physico-chemical properties. *Energy Sources, Part A: Recovery, Utilization, and Environmental Effects,* 38(11), 1530–1536; doi.org/10.1080/15567036.2014.953713

Prasara-A, J., Gheewala, S.H. (2017). Sustainable utilization of rice husk ash from power plants: A review. *Journal of Cleaner Production, 167*, 1020-1028; doi.org/10.1016/ j.jclepro.2016.11.042

Quiroga, E., Molto, J., Conesa, J.A., Valero, M.F., Cobo, M. (2020). Kinetics of the catalytic thermal degradation of Sugarcane residual biomass over Rh-Pt/CeO2-SiO2 for syngas production. *Catalysts, 10, 508*, 1-20; doi.org/10.3390/ catal10050508.

Rasool, T., Srivastava, V.C., Khan, M.N.S. (2018). Kinetic and thermodynamic analysis of thermal decomposition of Deodar (*Cedrus Deodara*) saw dust and rice husk as potential feedstock for pyrolysis. *International Journal of Chemical Reactor Engineering*, 20170184; doi: 10.1515/ijcre-2017-0184.

Rei, M.H, Yang, S.J., and Hong, C.H. (1986). Catalytic gasification of rice hull and other biomass. The general effect of catalyst. *Agricultural Wastes, 18*, 269-281; doi.org/ 10.1016/0141-4607(86)90072-7

Rong, C., Li, B., Liu, W., Zhao, N. (2018). The effect of oyster shell powder & rice husk ash on the pyrolysis of rice husk for bio-oil. *Energy Sources Part A: Recovery, Utilization, and Environmental Effects, 40*(11), 1291-1304; doi.org/10.1080/ 15567036.2018.1469690

Sahraei, O.A.Z., Larachi, F., Abatzoglou, N., & Iliuta, M. C. (2017). Hydrogen production by glycerol steam reforming catalyzed by Ni-promoted Fe/Mg-bearing metallurgical wastes. *Applied Catalysis B: Environmental, 219*, 183–193; doi.org/10.1016/j.apcatb.2017.07.039

Said, M.M., John, G.R., Mhilu, C.F. (2014). Thermal charactheristics and kinetics of rice husk for pyrolysis process. *International Journal of Renewable Energy Research,*

4 (2), 275-278; www.ijrer.org/ijrer/index.php/ijrer/article/view/1120.

Salman, C.A., Naqvi, M., Thorin, E., and Yan, J. (2018). Gasification process integration with existing combined heat and power plants for poly-generation of dimethyl ether or methanol: A detailed profitability analysis. *Applied Energy, 226*, 116-128; doi.org/ 10.1016/j.apenergy.2018.05.069

Sarkar, J.K. and Wang, Q. (2020). Characterization of pyrolysis products and kinetic analysis of waste Jute Stick biomass. Processes, 8, 837; doi:10.3390/pr8070837

Shen, Y., Zhao, P., Ma, D., Yoshikawa, K. (2014a). Tar in-situ conversion for biomass gasification via mixing-simulation with rice husk char-supported catalysts. *Energy Procedia, 61*, 1549-1552; doi.org/10.1016/j.egypro.2014.12.167

Shen, Y., Zhao, P., Shao, Q., Ma, D., Takahashi, F., Yoshikawa, K. (2014b). In-situ catalytic conversion of tar using rice husk char-supported nickel-iron catalysts for biomass pyrolysis/gasification. *Applied Catalysis B: Environmental, 152-153*, 140-151; doi.org/10.1016/j.apcatb.2014.01.032

Shen, Y., Zhao, P., Shao, Q., Takahashi, F., Yoshikawa, K. (2015). In-situ catalytic conversion of tar using rice husk char/ash supported nickel-iron catalysts for biomass pyrolytic gasification combined with the mixing-simulation in a fluidized-bed gasifier. *Applied Energy, 160*, 808-819; doi.org/10.1016/j.apenergy.2014.10.074

Slopiecka, K., Bartocci, P., Fantozzi, F. (2012). Thermogravimetric analysis and kinetic study of poplar wood pyrolysis. *Applied Energy, 97*, 491-497; doi.org/10.1016/j.apenergy.2011.12.056

Thakkar, M., Makwana, J.P., Mohanty, P., Shah, M., Singh, V. (2016). In bed catalytic tar reduction in the auto-thermal fluidized bed gasification of rice husk: Extraction of silica, energy and cost analysis. *Industrial Crops and Products, 87*, 324-332; doi.org/10.1016/j.indcrop.2016.04.031

Turmanova, S. (2008). Non-isothermal degradation kinetics of filled with rise husk ash polypropene composites. Express Polym. Lett.; doi.org/ 10.3144/expresspolymlett.2008.18

Vyazovkin, S. (2021). Determining preexponential factor in model-free kinetic methods: How and Why?. *Molecules, 26*, 3077; https://doi.org/10.3390/molecules26113077

Wang, S-W, Li, D-X., Ruan, W-B., Jin, C-L., and Farahani, M.R. (2018). A techno-economic review of biomass gasification for production of chemicals. *Energy Sources, Part B: Economics, Planning, and Policy, 13*(8), 351-356; doi.org/10.1016/j.egypro.2017.03.1111

Wang, Z. & Xiong, Y. (2020). Simultaneous improvement in qualities of bio-oil and syngas from catalytic pyrolysis of rice husk by demineralization. *Energy Sources, Part A: Recovery, Utilization, and Environmental Effects* (Article in press); doi.org/10.1080/15567036.2020.1824038.

Widiyannita, A.M., Pradana, Y.S., Cahyono, R.B., Sutijan, Akiyama, T., Budiman, A. (2020). Kinetic study of pyrolysis of Ulin wood residue using thermogravimetric analysis. *International Journal on Anvanced Science Engineering Information Technology, 10 (4)*, 1624-1630; doi.org/10.18517/ijaseit.10.4.3640

Xiang, Z., Liang, J., Morgan, H.M., Liu, Y., Mao, H., BU., Q. (2018). Thermal behavior and kinetic study for co-pyrolysis of lignocellulosic biomass with polyethylene over Cobalt modified ZSM-5 catalyst by thermogravimetric analysis. *Bioresources Technology, 146*, 485-493; doi.org/10.1016/j.biortech.2017.09.178

Xu, Y., and Chen, B. (2013). Investigation of thermodynamic parameters in the pyrolysis conversion of biomass and manure to biochars using thermogravimetric analysis. *Bioresources Technology, 146*, 485–493; doi.org/10.1016/j.biortech.2013.07.086

Yan, J., Jiao, H., Li, Z., Lei, Z, Wang, Z., Ren, S., Shui, H., Kang, S., Yan, H., Pan, C. (2019). Kinetic analysis and modeling of coal pyrolysis eith model-free methods. *Fuel, 241*, 382-391; https://doi.org/10.1016/j.fuel.2018.12.079

Yoon, S.J., Son, Y.I, Kim, Y.K., and Lee, J.G. (2012). Gasification and power generation characteristics of rice husk and rice husk pellet using a downdraft fixed-bed gasifier. *Renewable Energy, 42*, 163-167; doi.org/10.1016/j.renene.2011.08.028

Yuan, R. and Shen, Y. (2019). Catalytic pyrolysis of biomass-plastic wastes in the presence of MgO and MgCO3 for hydrocarbon-rich oils production. *Bioresources Technology, 293*, 122076; doi.org/10.1016/j.biortech.2019.122076

Yuan, R., Yu, S., Shen, Y. (2019). Pyrolysis and combustion kinetics of lignocellulosic biomass pellets with calcium-rich wastes from agroforestry residues. *Waste Management, 87*, 86-96; doi.org/10.1016/j.wasman.2019.02.009

Yudiartono, A., Sugiyono, A., Wahid, L.M.A., Adiarso. (2018). Indonesia Energy Outlook 2018, Sustainable Energy for Land Transportation. *Center of Assessment for Process and Energy Industry - Agency for the Assessment and Application of Technology*, Jakarta, Indonesia. ISBN 978-602-1328-05-7. www.bppt.go.id